Theor Chem Acc (2001) 105:219–226
DOI 10.1007/s002140000206

Theoretical
Chemistry Accounts

Regular article

Quasirelativistic valence ab initio calculation of the potential-energy curves for Cd–rare gas atom pairs

E. Czuchaj[1], **M. Krośnicki**[1], **H. Stoll**[2]

[1] Institute of Theoretical Physics and Astrophysics, University of Gdańsk, ul. Wita Stwosza 57, 80-952 Gdańsk, Poland
[2] Institut für Theoretische Chemie, Universität Stuttgart, Pfaffenwaldring 55, 70550 Stuttgart, Germany

Received: 20 April 2000 / Accepted: 1 September 2000 / Published online: 21 December 2000

Abstract. The results of large-scale valence ab initio calculations of the potential-energy curves for the ground states and several excited states of Cd–rare gas (RG) van der Waals molecules are reported. In the calculations, Cd^{20+} and RG^{8+} cores are simulated by energy-consistent pseudopotentials, which also account for scalar-relativistic effects and spin-orbit interaction within the valence shell. The potential energies of the Cd–RG species in the ΛS coupling scheme have been evaluated by means of ab initio complete-active-space multiconfiguration self-consistent-field (CASSCF)/CAS multireference second-order perturbation theory (CASPT2) calculations with a total 28 valence electrons, but the spin-orbit matrix has been computed in a reduced configuration interaction space restricted to the CASSCF level. Finally, the Ω potential curves are obtained by diagonalization of the modified spin-orbit matrix (its diagonal elements before diagonalization substituted by the corresponding CASPT2 eigenenergies). The calculated potential curves, especially the spectroscopic parameters derived for the ground states and several excited states of the Cd–RG species are presented and discussed in the context of available experimental data. The theoretical results exhibit very good agreement with experiment.

Key words: Collision complexes – Pseudopotentials – Potential curves

1 Introduction

Weakly bound complexes of atoms and small molecules have become the subject of numerous spectroscopic studies in recent years. A great deal of spectroscopic and dynamical information has been accumulated concerning the van der Waals molecules formed of a group IIb metal atom and a rare-gas (RG) atom in the ground and excited states of the former. Detailed information derived from experimental measurements on these species provides a better understanding of van der Waals bonding as well as interatomic potentials. The latter are important for interpretation of various dynamical processes, such as collisional redistribution of resonance radiation, electronic energy transfer, "orbital-following" interpretation of polarization effects in energy-transfer collisions, as well as "half-collision" experiments involving excitation of van der Waals molecules. Most of the interatomic potentials for the group IIb metal–RG species are derived from studies of the profiles of the metal atom intercombination ($^3P_1 - {}^1S_0$) and resonance ($^1P_1 - {}^1S_0$) lines broadened by RGs as well as the associated satellite bands which appear in the absorption and/or emission spectra. To derive the potential parameters from the observed absorption and/or emission spectra a data inversion technique based on the quasistatic theory of line broadening has been used [1–3]. In recent years, the supersonic free expansion technique was utilized to produce a variety of weakly bound metal atom–RG van der Waals molecules. This technique in combination with "pump and probe" methods of laser spectroscopy was successfully used in studies of metal atom–RG molecules in many laboratories [4–13]. Laser excitation spectra of these species were subjected to rovibrational analysis, which yielded spectroscopic parameters for the ground (X^10^+) and several excited states. Spectroscopic data derived from these experiments also permit a straightforward verification of theoretical interatomic potentials.

However, the theoretical potentials for the group IIb–RG species are still known insufficiently, in spite of substantial progress in both theory and experiment. So far three theoretical reports have appeared on the calculation of the Cd–RG potentials. In the first study [14], *l*-independent statistical pseudopotentials were used to simulate both the Cd core and RG atoms and the calculations involved only diatomics with heavy RG atoms (Ar, Kr, Xe). For complexes with light RG atoms (He, Ne)

Correspondence to: E. Czuchaj
e-mail: czu@iftia.univ.gda.pl

molecular calculations were performed with more accurate l-dependent pseudopotentials at the valence self-consistent-field (SCF)/configuration interaction (CI) level [15]. Unfortunately, available experimental data on the Cd–RG complexes deviate considerably from those theoretical results. We ascribed that discrepancy primarily to a too simplified treatment of the RG atoms in Refs. [14, 15], where they were entirely replaced by pseudopotentials supplemented with polarization potentials. On the other hand, taking into account the valence electrons of the RG atoms explicitly should certainly improve the description of the Cd–RG Pauli repulsion and better account for polarization effects of the RG atoms on Cd. As a consequence, in our last work on Cd–RG species [16], the Cd and RG atoms were considered, respectively, as two- and eight-valence electron systems, whereas the Cd^{2+} and RG^{8+} cores were replaced by scalar-relativistic energy-consistent pseudopotentials. In the case of Cd, a core-polarization potential was added in order to account for core–valence correlation contributions. Additionally, the potential curves computed were split into spin-orbit (SO) components in a semiempirical manner following the "atoms-in-molecules" model. Comparison of the spectroscopic parameters derived with available experimental values indicated rather good agreement of theory with experiment.

In view of recent improvements in the applied software (MOLPRO) [17], we have undertaken new molecular calculations on the group IIb–RG complexes, with the aim of removing the still existing deficiencies in the theory. The present work is a part of our systematic study of the interaction potentials of collisionally formed van der Waals molecules. Since fully ab initio calculations of molecular structure require high computational effort for atoms such as Cd and heavy RGs, an approach in which only the valence electrons of the interacting atoms are treated explicitly and atomic cores are simulated by l-dependent pseudopotentials still seems justified. In contrast to our previous calculations [16], however, the Cd atom is treated as a 20-valence electron system in the present approach, and the Cd^{20+} and RG^{8+} cores are substituted by ab initio scalar-relativistic energy-consistent pseudopotentials supplemented by the corresponding SO operators.

In this article, we present results concerning the potential-energy curves of the Cd–RG complexes. After a short presentation of the theory and the technical details of the calculations given in Sect. 2, the results obtained are discussed in the context of available experimental data in Sect. 3.

2 Method

2.1 General formulation

The calculation of the adiabatic energies $E_i(R)$ between a group IIb atom (A) and a RG atom (B) in the Born–Oppenheimer approximation reduces to the solution of the Schrödinger equation

$$(H_A + H_B + V_{AB})\Psi_i(\mathbf{x},\mathbf{R}) = E_i(R)\Psi_i(\mathbf{x},\mathbf{R}) \ , \tag{1}$$

where H_A and H_B are the Hamiltonians of the isolated atoms A and B, V_{AB} stands for the interaction between the two atoms, $\mathbf{x}$ represents the electronic coordinates, while $\mathbf{R}$ is the position vector of B relative to A. In the present approach the *nsnpnd* core electrons and $(n+1)s$ $(n=4)$ valence electrons of atom A are considered on an equal footing. Consequently, the 20 valence electrons of atom A and the eight valence electrons of atom B are treated explicitly, while the A^{20+} and B^{8+} cores as well as valence-shell scalar-relativistic effects and SO interaction are represented by lj-dependent quasirelativistic pseudopotentials. The valence model Hamiltonian in Eq. (1) can be written (in atomic units) as

$$H = -\frac{1}{2}\sum_i \Delta_i + V_{av} + V_{so} + \sum_{j>i=1}^{N}\frac{1}{r_{ij}} + \sum_{\lambda>\mu}\frac{Q_\lambda Q_\mu}{r_{\lambda\mu}} \ , \tag{2}$$

where i,j denote valence electrons, λ,μ are core indices and Q_λ, Q_μ represent core charges. The SO-averaged pseudopotential, V_{av}, which accounts for scalar-relativistic effects, has the following semilocal form

$$V_{av} = -\sum_{\lambda,i}\frac{Q_\lambda}{r_{\lambda i}} + \sum_{\lambda,i}\sum_{l,k} A_{\lambda lk}\exp(-a_{\lambda lk}r_{\lambda i}^2)P_{\lambda l} \ , \tag{3}$$

where $P_{\lambda l}$ is the projection operator onto the Hilbert subspace of angular symmetry l with respect to core λ

$$P_{\lambda l} = \sum_{m=-l}^{l} |\lambda lm><\lambda lm| \ . \tag{4}$$

In turn the pseudopotential representing the SO operator takes the form

$$V_{so} = \sum_{\lambda,i}\sum_{l}\frac{2\Delta V_{i,\lambda l}}{2l+1}P_{\lambda l}\boldsymbol{l}_i\boldsymbol{s}_i P_{\lambda l} \ . \tag{5}$$

The difference $\Delta V_{i,\lambda l}$ of the radial parts of the two-component quasirelativistic pseudopotentials $V_{\lambda l,l+1/2}$ and $V_{\lambda l,l-1/2}$ is written similarly to the radial part of the SO-averaged pseudopotential, V_{av} in terms of Gaussian functions

$$\Delta V_{i,\lambda l} = \sum_k \Delta A_{\lambda lk}\exp(-a_{\lambda lk}r_{\lambda i}^2) \ . \tag{6}$$

In the case of small-core pseudopotentials the polarization potential which describes, among others, core–valence correlation effects, is usually disregarded, because the dipole polarizabilities of the cores are small. The last term in Eq. (2) represents the core–core interaction. Since the A^{20+} and B^{8+} cores are well separated, we chose a simple point-charge Coulomb interaction in the latter case.

2.2 Details of calculations

High-level valence ab initio calculations were carried out for the ground states and several excited states of Cd–RG species. As mentioned earlier, the Cd and RG atoms in the present approach are treated, respectively, as 20-valence and eight-valence electron species. The free parameters occurring in V_{av} and V_{so}, defined by Eqs. (3), (5) and (6), for the Cd atom were taken from Ref. [18]. The corresponding optimized primitive (8s7p6d) basis set was used [18], augmented with one diffuse s, p and d function (exponents 0.006282, 0.012638, 0.025128, respectively). A polarization set of four f functions (exponents 4.5, 1.5, 0.5, 0.17) and two g functions (exponents 1.5, 0.5) [19] was added. The final basis set can be designated as (9s8p7d4f2g)/[8s7p6d4f2g]. The quality of the present 20-valence electron model of the Cd atom, including SO coupling, was verified in atomic CI calculations for the ground state and several excited states. First SO-averaged energies were calculated in the LS coupling scheme for all the states from $(5s^2)\ ^1S$ up to the $(6s)^1S$ Rydberg state on the basis of complete-active-space multiconfiguration self-consistent-field (CASSCF) calculations followed by CAS multireference second-order perturbation theory (CASPT2) calculations. The 20 valence electrons of the Cd atom were distributed among the 4s4p4d outer core and 5s5p valence as well as the 6s6p Rydberg orbitals to form the active space in the D_{2h} point group. The 4s4p4d orbitals were kept doubly occupied in all configuration state functions (CSFs). They were fully optimized in multiconfiguration (MC)SCF calculations and correlated through single and double excitations from the reference CSFs in the

CASPT2 calculations. On the other hand, the SO matrix was restricted to the MCSCF level. However, to account for scalar relativistic effects and correlation contributions at a higher level of theory, the diagonal elements of the SO matrix before diagonalization were substituted for the corresponding CASPT2 eigenenergies. The calculated excitation energies for Cd from the $(5s^2)^1S$ ground state to the $(5p)^3P_0$, $(5p)^3P_1$, $(5p)^3P_2$ and $(5p)^1P_1$ states amount, respectively, to 30220 (30114), 30685 (30656), 31634 (31826) and 44784 (43692) cm^{-1}. The numbers in parentheses denote the experimental values [20]. Correspondingly, for the $(6s)^3S$ and $(6s)^1S$ Rydberg states one gets 51863 (51484) and 52759 (53310) cm^{-1}.

In turn, the one-component relativistic energy-consistent ab initio pseudopotentials for the RG atoms Ne to Xe, supplemented with effective SO potentials, were taken from Nicklass et al. [21]. In the case of He, the contracted (13s8p5d3f)/[7s8p5d3f] basis set has s functions taken from Ref. [22], p and d functions (exponents 9.88, 3.952, 1.5808, 0.63232, 0.252928, 0.101171, 0.040468, 0.016187 and 0.7584, 0.30336, 0.121344, 0.048538, 0.019415, respectively) derived from Ref. [23] and f functions (exponents 5.411, 1.707, 0.5345) taken from the augmented correlation-consistent polarized valence quintuple-zeta basis set of Ref. [24]. On the other hand, for Ne, Ar, Kr and Xe we started with the optimized uncontracted basis sets taken from Nicklass et al. [21] (7s7p3d for Ne, 6s6p3d otherwise). These basis sets were augmented with two diffuse s functions (exponents 0.124, 0.05), two p functions (0.089, 0.036) and one d function (0.088) for Ne, three s functions (0.057726, 0.025359, 0.011141), two p functions (0.039397, 0.016321) and one d function (0.04) for Ar, three s functions (0.065356, 0.024811, 0.009419), two p functions (0.041501, 0.015833) and one d function (0.0616) for Kr, and three s functions (0.033561, 0.015814, 0.007451), two p functions (0.022045, 0.010345) and one d function (0.062845) for Xe. The diffuse exponents were determined by means of even-tempered continuation of the series of low exponents in each case. In addition, for Ne and Ar we added the 3f augmented correlation consistent polarized valence quintuple-zeta set from Ref [24]. In turn, for Kr and Xe we added, respectively, four f functions (exponents 2.703594, 0.3225, 0.1409, 0.0616) and three f functions (2.434884, 0.5111866, 0.10732) derived from Ref. [25]. The two f functions with the largest exponents for Kr were contracted with contraction coefficients 0.019361 and 0.540751, respectively. Finally, we used the uncontracted (9s9p4d3f) basis set for Ne and a contracted [8s7p4d3f] basis for the remaining RG atoms.

The potential-energy curves were first evaluated on the basis of CASSCF calculations followed by CASPT2 calculations with an open-shell correction term to the one-electron Fock operator as proposed by Werner [26]. The active space is spanned by the molecular counterparts of the Cd 5s5p and 6s6p orbitals in the C_{2v} point group. [It turns out that taking into account the Cd 6p orbitals in the calculations substantially improves agreement of the calculated Cd (5s5p) ^3P and ^1P atomic energies with the experimental values]. The molecular orbitals used in the calculations were determined in a state-averaged CASSCF for the ground and excited states together. The valence orbitals of the RG atom and the 4s4p4d orbitals of Cd were kept doubly occupied in all CSFs; however, they were fully optimized in the CASSCF calculations and correlated through single and double excitations from the reference configurations in the multireference perturbation calculations (CASPT2).

The next step in the calculations involves the inclusion of SO coupling at the CI level. In the present approach the SO matrix elements are computed using the SO pseudopotentials for both Cd and RG atoms. The SO eigenstates are obtained by diagonalizing the $H_{el} + H_{so}$ matrix in a basis formed of selected spatial configurations multiplied with appropriate spin functions. The resulting products are grouped together according to symmetry to form an appropriate matrix for each of the four C_{2v} double group representations. In the present calculations the off-diagonal elements of the SO operator are computed by employing the truncated version of the CI space restricted to the CASSCF wavefunctions. However, to account for correlation effects at a higher level of theory, the diagonal elements of the SO matrix before diagonalization were replaced by the precomputed CASPT2 eigenenergies.

It has been found that the basis-set superposition error (BSSE) is appreciable in the present calculations and it cannot be neglected if the calculated potential curves are to be used in a detailed discussion of the observed Cd–RG spectra. BSSE was eliminated using the standard counterpoise method [27]. The correlated calculations were performed using the MOLPRO program code of Werner and Knowles [17].

3 Results and discussion

The molecular calculations were performed for the Cd–RG diatomics in the internuclear separation range from 3.5 to 40 a_0 with different step sizes. The calculations involve molecular states correlating with the Cd atomic states from the $(5s^2)^1S$ ground state up to the $(5s6s)^1S$ Rydberg state. The potential energies were calculated with respect to the energy of the separated atoms at $R = 100\ a_0$. "Large" SO matrices comprising all molecular states considered are formed according to symmetry and diagonalized for each case to yield the appropriate SO potential energies. The corresponding potential curves are displayed in Figs. 1–8. The numerical values of the calculated potential energies are available from the author (E.C.) upon request. Both the ground- and excited-state potentials are counterpoise-corrected, i.e., for each R value they were obtained by subtracting the sum of the corresponding Cd atomic SO energy and the

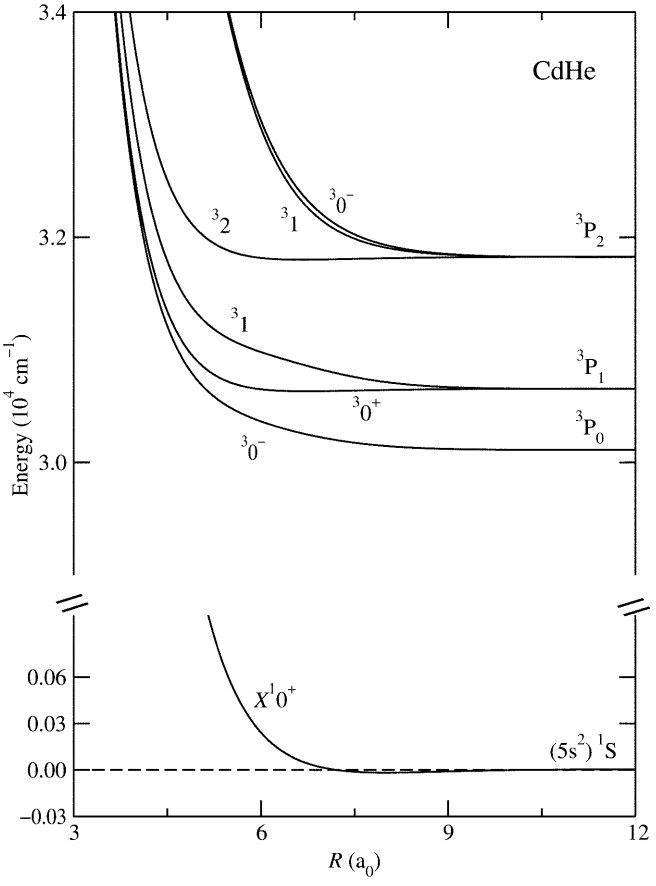

Fig. 1. Potential-energy curves of the CdHe electronic states correlating with the $Cd(5s5p^3P_J)$ atomic multiplet states and the $Cd(5s^2\ ^1S)$ ground state

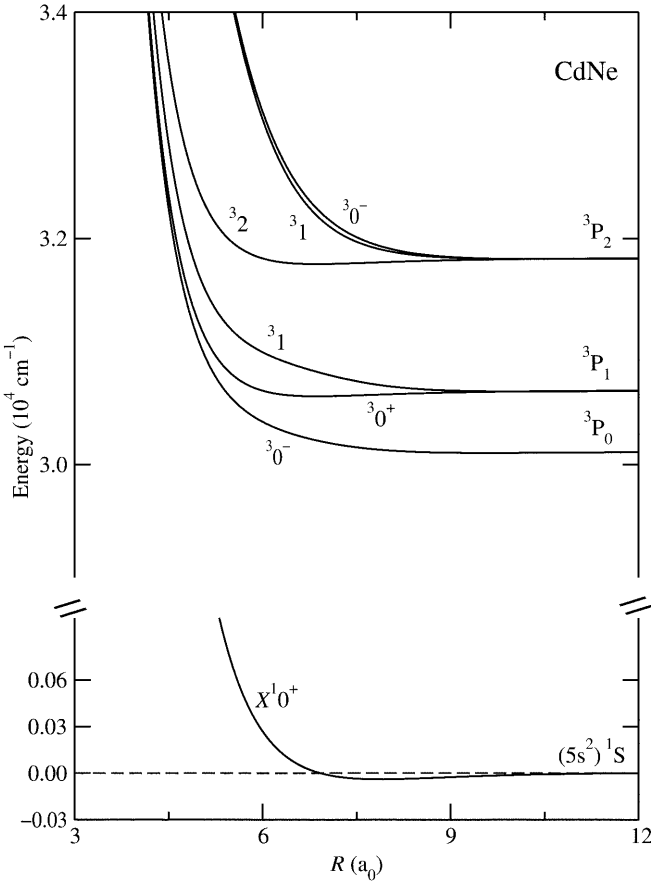

Fig. 2. Potential-energy curves of the CdNe electronic states correlating with the Cd(5s5p^{3}P$_J$) atomic multiplet states and the Cd(5s^2 ^{1}S) ground state

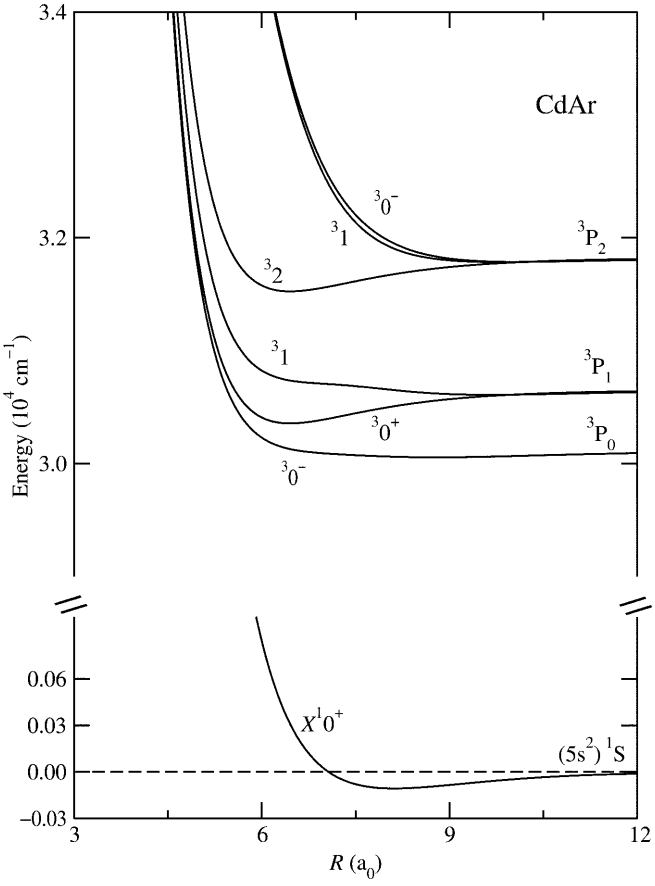

Fig. 3. Potential-energy curves of the CdAr electronic states correlating with the Cd(5s5p^{3}P$_J$) atomic multiplet states and the Cd(5s^2 ^{1}S) ground state

ground-state RG energy calculated individually in the molecular basis from the proper molecular energy. The counterpoise correction of the BSSE is found to reduce substantially the binding energy of both the ground- and excited-state potentials of the Cd–RG molecules, but it increases the bond lengths only slightly. In any case, a theoretical determination of reliable spectroscopic parameters for the Cd–RG species has to take into account the BSSE. Figures 1–5 display the Ω potential curves correlating to the Cd(5s^2 ^{1}S) ground state and the Cd(5s5p ^{3}P$_J$) triplet states for the Cd–RG pairs. Owing to a large energy gap (31246 cm^{-1}) between the triplet state and the ground state of the Cd atom, the influence of the SO interaction on the ground-state potential is of minor importance; however, the SO interaction becomes important for the Ω states correlating with different fine-structure components of the Cd(5s5p) triplet state. As a result, the ground state for all Cd–RG species is almost exclusively the $X^1\Sigma^+$ state, especially at larger R values. On the other hand, the $A^3\Pi$ and $B^3\Sigma^+$ states mix by SO interaction to yield the appropriate Ω states. The contribution arising from the upper singlet (5s5p)^{1}P state to the triplet states proves to be insignificant. As seen, all potential curves in Figs. 1–5 change regularly with internuclear separation. In general, there is no qualitative difference between them and the corresponding potential curves calculated by us earlier [16], where the two-valence electron model for the Cd atom was used and molecular SO coupling was treated as R-independent. As a rule, the bond strengths of the Cd–RG molecules increase regularly with the polarizabilities of the RG atoms going from He to Xe. The only possible long-range attractive force between the two atoms is due to the dispersion interaction caused by correlations between the fluctuating multipolar charge distributions of the atoms. At a shorter R range, with decreasing internuclear separation the attraction is overcome owing to strong repulsion resulting from the overlap of the electron distributions of the two atoms (Pauli repulsion). For the ground state the corresponding equilibrium position (R_e) slightly increases with the RG atom size except for He, for which R_e is somewhat greater than for Ne. The lowest excited state correlates to the ^{3}P$_0$ state of the Cd atom. The corresponding ^{3}0$^-$ potential curve changes regularly with R and possesses a shallow minimum at an internuclear separation shorter than that for the $X^1$0$^+$ ground state. The bonding energy of the potential curve increases on going from He to Xe. Two molecular states correlate to the Cd ^{3}P$_1$ state. One of them, labeled $A^3$0$^+$, becomes a nearly pure $^3\Pi$ state owing to the relatively large single-triplet energy gap. The second state, labeled $B^3$1, interacts mainly with the higher lying $^3\Sigma$ state correlating to the Cd ^{3}P$_2$ state owing to SO mixing. As a consequence, the $A^3$0$^+$ state is

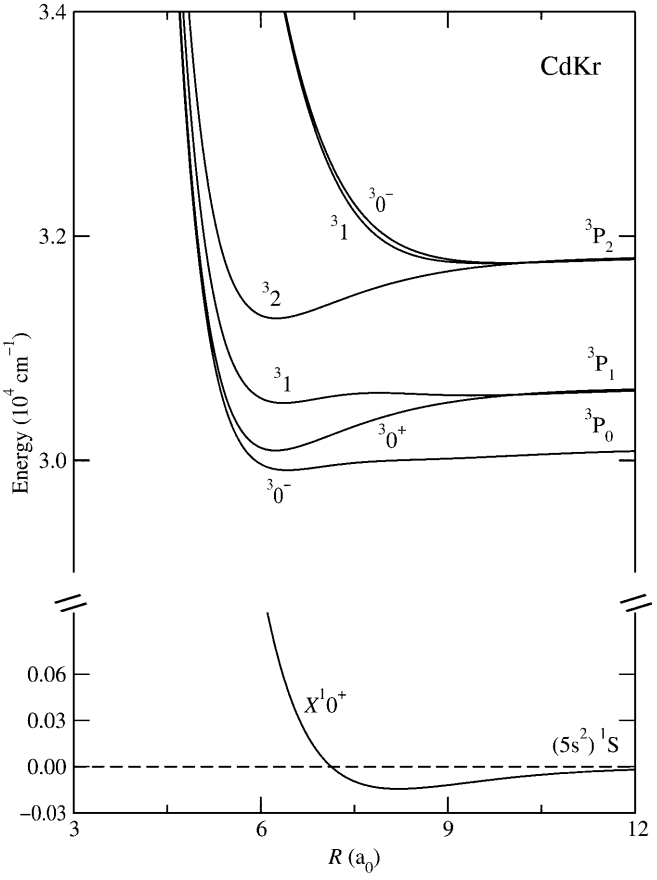

Fig. 4. Potential-energy curves of the CdKr electronic states correlating with the Cd(5s5p^{3}P$_J$) atomic multiplet states and the Cd(5s^2 ^{1}S) ground state

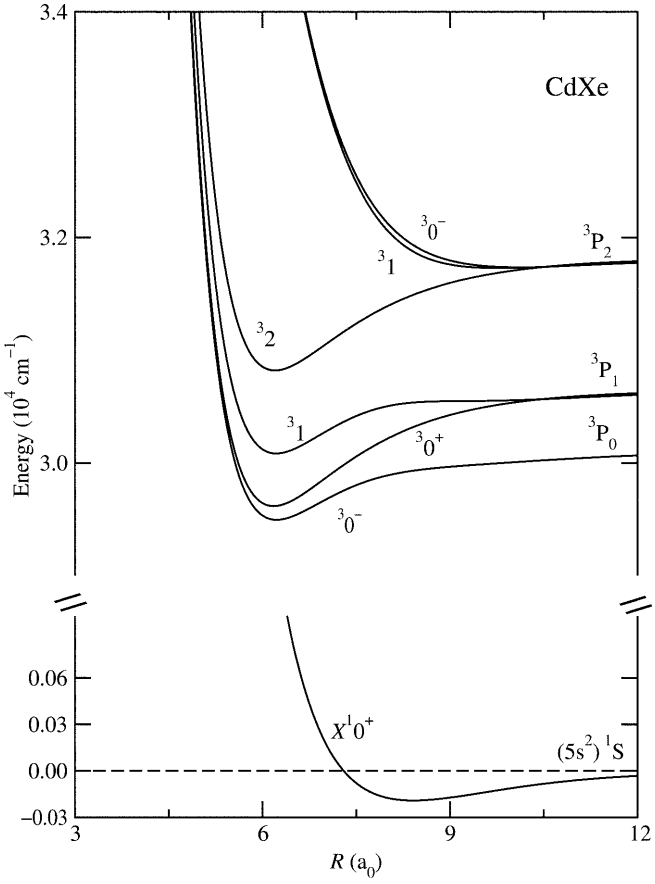

Fig. 5. Potential-energy curves of the CdXe electronic states correlating with the Cd(5s5p^{3}P$_J$) atomic multiplet states and the Cd(5s^2 ^{1}S) ground state

much deeper than the ground $X^1 0^+$ state, while exactly the reverse is true for the $B^3 1$ state.

In turn three molecular states correlate to the Cd $^3P_2$ state. The most attractive of them, labeled $^3 2$, becomes a pure $^3\Pi$ state because there is no other molecular state with the same quantum number, Ω, to interact. The remaining two states, $^3 1$ and $^3 0^-$, exhibit a repulsive character with weak attraction at larger R and increasing bonding energy on going from He to Xe. The most interesting result of the present calulations is the shape of the $B^3 1$ potential curves for different RGs. This is illustrated in Fig. 6. As seen from the figure, the shape of the $B^3 1$ potential curve for CdHe and CdNe varies regularly with R; however, the potential shape alters dramatically for the remaining RGs. In particular, the $B^3 1$ potential curve for CdKr possesses two minima. The inner potential well with the bonding energy $D_e = 145\,\mathrm{cm}^{-1}$ and $R_e = 6.37\,a_0$, which is the result of SO interaction, is separated from the outer shallower potential well ($D_e = 77\,\mathrm{cm}^{-1}$, $R_e = 9.38\,a_0$) by a small potential barrier located at about $8.0\,a_0$. Although this effect has not yet been observed directly in experiment, since electronic transitions from the CdKr ground state to vibronic states of the deeper $B^3 1$ potential well do not occur ($R_e'' \gg R_e'$), some suggestions for a double minimum of the CdKr $B^3 1$ potential curve have recently been made. This unexpected result of the present calculations is believed to be of major importance for the interpretation of the corresponding Cd–heavy RG electronic-vibrational spectra based currently on the assumption that both the potentials involved in an electronic transition are well represented by the Morse function.

Two Ω states ($^1 0^+$, $^1 1$) correlate to the (5s5p) ^{1}P state of the Cd atom. Owing to the only weak interaction with nearby states of the same symmetry, these states become almost pure $^1\Sigma$ and $^1\Pi$ states. In the case of the $^1\Sigma$ state the shielding of the metal atom core is yet greater than in the ground state owing to the larger on-axis electron density, which leads to a weakening of the attractive interaction. As a consequence, the corresponding potential is strongly repulsive with a very shallow minimum lying at a larger R. On the other hand, the electrostatic attraction in the excited $(5p)^1\Pi$ state is considerably stronger compared to that in the ground state. This is undoubtedly due both to the diffuse nature of the Cd 5p orbitals and their perpendicular orientation with respect to the bond axis. As a result, the Cd atom core exposed to the RG atom increases the charge-induced multipole interaction. The corresponding potential curves are displayed in Fig. 7. Finally, the potential curves correlating to the $(6s)^3$S and $(6s)^1$S Cd states are shown in Fig. 8. In general, for each Cd–RG molecule the singlet potential curves are somewhat deeper than the corresponding triplet ones. The corresponding potentials for CdHe and

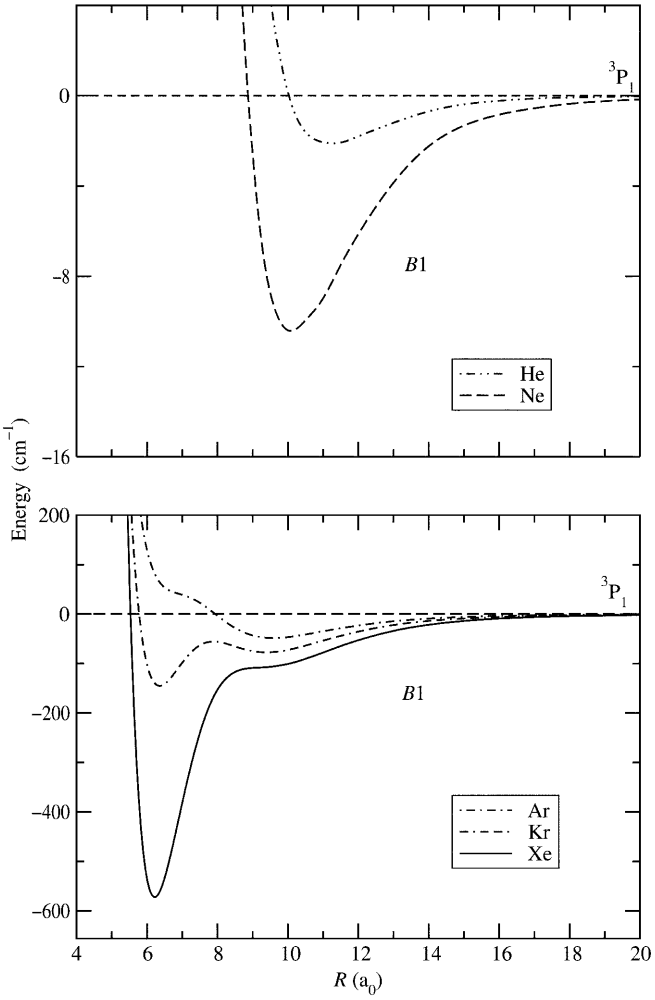

Fig. 6. Potential energy curves (B1) for the Cd–rare gas (*RG*) electronic states correlating with the Cd($5s5p^3P_1$) atomic state

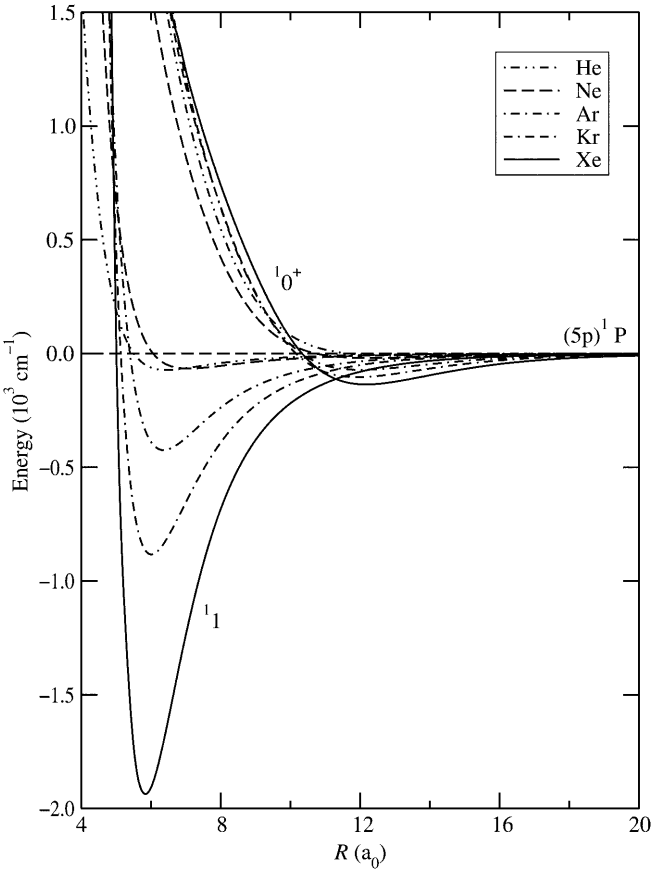

Fig. 7. Potential energy curves for the Cd–RG electronic states correlating with the Cd($5s5p^1P$) atomic state

CdNe are entirely repulsive. They exhibit some humps when going towards smaller internuclear distances. The humps go over into shallow minima at yet shorter internuclear separations. For heavier RG atoms the potential curves in question become attractive with decreasing R. Their bonding energies increase on going from Ar to Xe. The apparent difference in the potential well depth of the singlet and triplet states originates mainly from different spatial distributions of the Cd valence electron density in both these multiplets. The potential well depths, D_e, and the equilibrium positions, R_e, of the potential curves were extracted using a cubic spline approximation of the calculated potentials near their equilibrium positions. In addition, the radial Schrödinger equation for nuclear motion was solved numerically with the calculated potentials to evaluate the corresponding vibrational levels and, hence, the fundamental frequencies, ω_e, which thus also contain anharmonic effects. The derived spectroscopic parameters D_e, R_e and ω_e for the most important potentials of the Cd–RG molecules are summarized in Table 1. They are also compared with both the existing experimental values and the former theoretical results [16]. As seen, the difference between the two sets of theoretical results is not too much. Except for CdHe, the present potentials exhibit, in general, better agreement with experiment than the former theoretical results. The most striking difference is seen in the case of the B^31 bonding energies for CdKr and CdXe, but one has to remember that the experimental values of D_e were determined assuming the Morse function to be an adequate representation of this potential.

Several experimental studies revealed some satellites in the absorption profile of the Cd intercombination line (326.1 nm) perturbed by RGs. Both the satellites in the red and the blue wing of the spectral line are attributed to electronic transitions from the $X0^+$ ground state to the B^31 and $A0^+$ states. According to the quasistatic theory of line broadening and the classical formulation of the Franck–Condon principle, extrema in the difference potentials are directly related to the positions of satellites in the corresponding spectral line. On the other hand, the so-called unified Franck–Condon theory of spectral line shape predicts line satellites somewhat closer to the line center in comparison to the classical satellites. The calculated ($B^31 - X0^+$) and ($A0^+ - X0^+$) difference potentials for CdAr and CdXe are displayed in Fig. 9. The $B^31 - X0^+$ difference potential for CdAr has a maximum of $115\,cm^{-1}$ at $R = 7.8\,a_0$ and, correspondingly, of $75\,cm^{-1}$ at $R = 8.7\,a_0$ for CdXe. In addition, the curves exhibit shallow minima of $12\,cm^{-1}$ at $R = 11.6\,a_0$ for CdAr and $22\,cm^{-1}$ at $R = 11.8\,a_0$ for

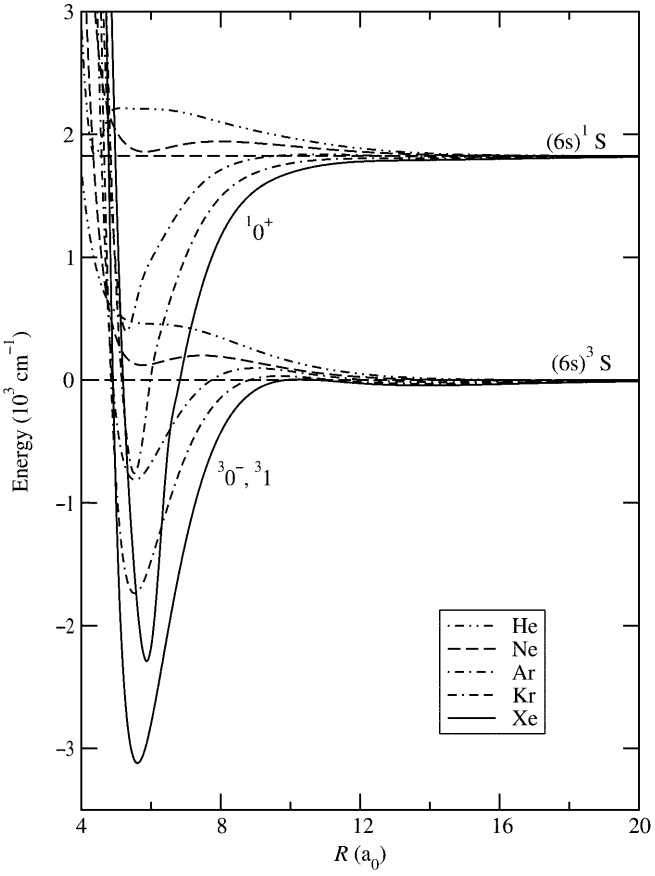

Fig. 8. Potential energy curves for the Cd–RG electronic states correlating with the Cd(5s6s^{3}S) and Cd(5s6s^{1}S) atomic states

CdXe. That means that the calculated potentials predict both the red and the blue satellites in the Cd intercombination line perturbed by Ar and Xe. This prediction is entirely in line with the experimental findings. Helmi et al. [2] observed the red satellite for CdXe at about 18 cm^{-1} and a wide blue satellite which extends from about 25 to 80 cm^{-1} from the line center. In turn, Roston et al. [3] measured the broad blue satellite for CdAr extending from about 40 to 130 cm^{-1} from the line center. It is interesting that in light of the present calculations only the B^{3}1 state is responsible for the appearance of both the blue and red satellites in the spectral line considered, whereas the A0$^+$ state contributes to the intensity distribution of the line only in the direct vicinity of the line center. Furthermore, the calculated ($5p\,^1P^1 0^+ - X0^+$) difference potential for CdKr exhibits a maximum of 1100 cm^{-1} at about $R = 6.7\,a_0$ which should correspond to a blue satellite in the Cd resonance line. Indeed, such a far-blue-wing satellite at about 825 cm^{-1} from the line center was observed by Bousquet in studies of the Cd resonance line perturbed by Kr [1]. The fact that the calculated potentials predict the satellites observed experimentally in the Cd spectral lines and the derived spectroscopic parameters summarized in Table 1 proves undoubtedly the reliability of the present results.

4 Conclusions

Potential-energy curves for the Cd–RG van der Waals molecules have been calculated at the valence CASSCF/CASPT2 level including SO interaction. The Cd^{20+} and

Table 1. Spectroscopic parameters D_e (cm^{-1}), R_e (bohr) and ω_e (cm^{-1}) for the X^{1}0$^+$, A^{3}0$^+$, B^{3}1, C$^1\Pi_1$ and D$^1\Sigma_0^+$ states of Cd–rare gas molecules. *Top row*-this work; *second row*-Ref. [16]

Molecule	X^{1}0$^+$			A^{3}0$^+$			B^{3}1			C$^1\Pi_1$			D$^1\Sigma_0^+$		
	D_e	R_e	ω_e	D_e	R_e	ω_e	D_e	R_e	ω_e	D_e	R_e	ω_e	D_e	R_e	ω_e
Cd–He	16.8	8.02	10.8	27.5	6.75	19.7	2.2	11.30	–	72	6.45	29.8	9.2	13.11	3.3
	15.1	8.50	10.0	36	6.75	19.5	7.8	10.50	4.8	75	6.50	35.6	–	–	–
	14.2[a]	8.18[a]	9.6[a]	41.2[a]	5.35[a]	20[a]	6.1[a]	8.41[a]	3.6[a]						
Cd–Ne	34	7.98	13.1	53	6.83	16.5	10	10.08	4.5	66	7.12	15.9	19.5	12.30	6.3
	55	7.80	15.2	115	6.50	25.8	28	9.60	8.8	111	6.60	23.7	2	15.10	–
	28.3[c]	8.14[c]		70.5[c]			9.6[c]			58.9[d]		23.4[d]			
Cd–Ar	107	8.11	18.3	324	6.37	37.1	48	9.62	9.1	451	6.30	40.6	71	12.02	9.6
	112	8.10	17.5	355	6.40	35.9	82	9.50	11.7	475	6.10	42.2	11.5	13.80	3.3
	107[e]	8.13[e]		325[e]			56[b]	9.47[b]		544[d]		48[d]			
Cd–Kr	145	8.20	16.6	568	6.24	40.2	145	6.37	30.2	883	6.05	48.5	103	11.92	9.2
	134	8.40	15.3	535	6.40	36.1	112	9.40	9.2	843	5.90	48.8	21	13.30	3.6
	130[f]	8.18[d]		529[e]			60.2[g]			1036[d]		56.7[d]			
Cd–Xe	192	8.41	16.8	1040	6.18	52	572	6.22	9.1	1936	5.83	70	136	12.18	9.3
	153	8.80	14	934	6.25	44.7	151	9.25	10	1750	5.85	69	36.5	13.10	4.2
	192[h]	8.09[h]		1086 ∓ 60[e]			152∓ 15[h]			2485[d]		87.7[d]			

[a] Ref. [13]
[b] Ref. [4]
[c] Ref. [28]
[d] Ref. [5]
[e] Ref. [7]
[f] Ref. [1]
[g] Ref. [10]
[h] Ref. [2]

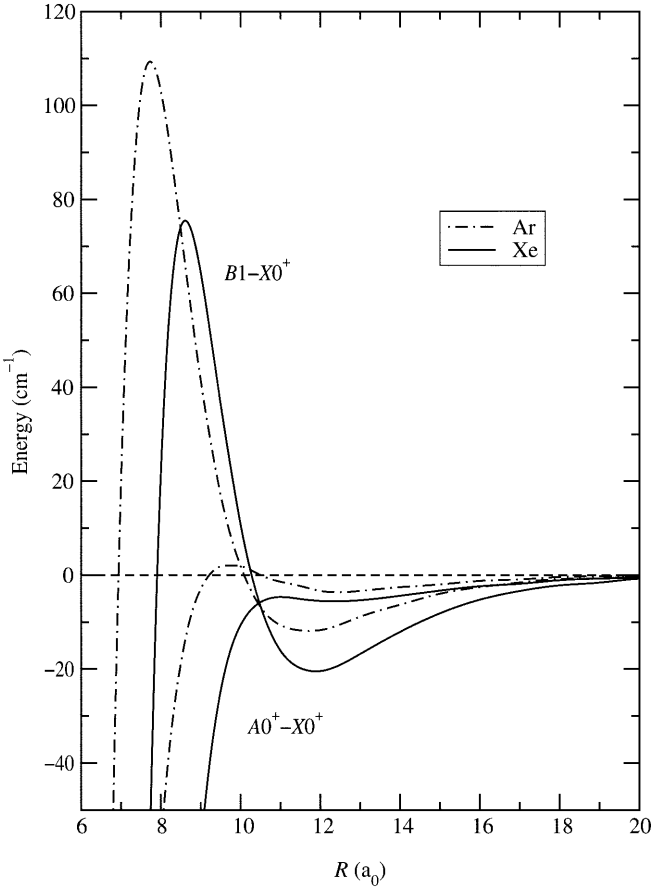

Fig. 9. Difference potentials $B1 - X0^+$ and $A0^+ - X0^+$ for CdXe and CdAr

RG^{8+} cores as well as scalar-relativistic effects and SO interaction were modeled by *lj*-dependent energy-consistent pseudopotentials. Very good agreement of theory with experiment has been obtained, especially for the ground states and the lower excited triplet states for all the Cd–RG combinations. This indicates that the 20-valence electron model of a group IIb metal atom along with explicitly taking into account the RG valence electrons in molecular structure calculations is appropriate for obtaining reliable potential curves for these diatomic species. The present results are believed to be helpful for both the identification and the better understanding of the observed electronic-vibrational spectra produced by the Cd–RG species.

Acknowledgements. This work was supported by the KBN under grant no. PB1124/P03/97/12. One of us (E.C.) wishes to thank W. Miklaszewski for his help with the numerical calculations.

References

1. Bousquet C (1986) J Phys B 19: 3859
2. Helmi MS, Grycuk T, Roston GD (1996) Chem Phys 209: 53
3. Roston GD, Helmi MS, Grycuk T (1996) Chem Phys 213: 365
4. Kowalski A, Czajkowski M, Breckenridge WH (1985) Chem Phys Lett 121: 217
5. Funk DJ, Kvaran A, Breckenridge WH (1989) J Chem Phys 90: 2915
6. Funk DJ, Breckenridge WH (1989) J Chem Phys 90: 2927
7. Kvaran A, Funk DJ, Kowalski A, Breckenridge WH (1989) J Chem Phys 89: 6069
8. Bennett R, Breckenridge WH (1992) J Chem Phys 96: 882
9. Bobkowski R, Czajkowski M, Krause L (1990) Phys Rev A 41: 243
10. Czajkowski M, Bobkowski R, Krause L (1991) Phys Rev A 44: 5730
11. Czajkowski M, Bobkowski R, Krause L (1992) Phys Rev A 45: 6451
12. Czajkowski M, Krause L, Bobkowski R (1994) Phys Rev A 49: 775
13. Koperski J, Czajkowski M (1998) J Chem Phys 109: 459
14. Czuchaj E, Sienkiewicz J (1984) J Phys B 17: 2251
15. Czuchaj E, Stoll H, Preuss H (1987) J Phys B 20: 1487
16. Czuchaj E, Stoll H (1999) Chem Phys 248: 1
17. (a) Werner H-J, Knowles PJ, with contributions from Amos RD, Berning A, Cooper DL, Deegan MJO, Dobbyn AJ, Eckert F, Hampel C, Hetzer G, Leininger T, Lindh R, Lloyd AW, Meyer W, Mura ME, Nicklass A, Palmieri P, Peterson K, Pitzer R, Pulay P, Rauhut G, Schütz M, Stoll H, Stone AJ, Thorsteinsson T, MOLPRO (a package of ab into programs). University of Brlmingham, UK; (b) Werner H-J, Knowles PJ (1985) J Chem Phys 82: 5053; (c) Knowles PJ, Werner H-J (1985) Chem Phys Lett 115: 259
18. Andrae D, Häussermann U, Dolg M, Stoll H, Preuss H (1990) Theor Chim Acta 77: 123
19. Dolg M, Flad H-J (1996) J Phys Chem 100: 6147
20. Moore CE (1958) Atomic energy levels (NSRDS-NBS circular no. 467). US GPO, Washington, DC
21. Nicklass A, Dolg M, Stoll H, Preuss H (1995) J Chem Phys 102: 8942
22. Behmenburg W, Makonnen A, Kaiser A, Rebentrost F, Stämmler V, Jungen M, Peach G, Devdariani A, Tserkovnyi S, Zagrebin A, Czuchaj E (1996) J Phys B 29: 3891
23. Rice JE, Taylor PR, Lee TJ, Almlöf J (1991) J Chem Phys 94: 4972
24. Woon DE, Dunning TH, Jr (1994) J Chem Phys 100: 2975
25. Maroulis G, Thakkar AJ (1988) J Chem Phys 89: 7320
26. Werner H-J (1996) Mol Phys 89: 645
27. Boys SF, Bernardi F (1970) Mol Phys 19: 553
28. Koperski J, Czajkowski M (2000) Eur Phys J D 10: 363